A coupled effect of nuclear and electronic energy loss on ion irradiation damage in lithium niobate

P. Liu [a,b], Y. Zhang [c,b,*], H. Xue [b], K. Jin [c], M.L. Crespillo [b], X. Wang [a], W.J. Weber [b,c]

[a]*School of Physics, State Key Laboratory of Crystal Materials & Key Laboratory of Particle Physics and Particle Irradiation (MOE), Shandong University, Jinan 250100, China*

[b]*Department of Materials Science & Engineering, University of Tennessee, Knoxville, TN 37996, USA*

[c]*Materials Science & Technology Division, Oak Ridge National Laboratory, Oak Ridge, TN 37831, USA*

*Corresponding author:

Email: *Zhangy1@ORNL.gov* Tel: *+001-865-574-8518*

Abstract

Understanding irradiation effects induced by elastic energy loss to atomic nuclei and inelastic energy loss to electrons in a crystal, as well as the coupled effect between them is a scientific challenge. Damage evolution of $LiNbO_3$ irradiated by 0.9 and 21 MeV Si ions at 300 K has been studied utilizing Rutherford backscattering spectrometry and channeling technique. During the low-energy ion irradiation process, damage accumulation produced due to elastic collisions is described utilizing a disorder accumulation model. Moreover, low electronic energy loss is shown to induce observable damage that increases with ion fluence. For the same electronic energy loss, velocity of the incident ion could affect the energy and spatial distribution of excited electron, and therefore effectively modify the diameter of the ion track.

Furthermore, nonlinear additivity phenomenon of irradiation damage induced by high electronic energy loss in pre-damaged $LiNbO_3$ has been observed. The result indicates that pre-existing damage induced from nuclear energy loss interacts synergistically with inelastic electronic energy loss to promote the formation of amorphous tracks and lead to rapid phase transformation, much more efficient than what is observed in pristine crystal solely induced by electronic energy loss. This synergistic effect is attributed to the fundamental mechanism that the defects produced by the elastic collisions result in decrease in thermal conductivity, increase in the electron-phonon coupling, and further lead to higher intensity in thermal spike from intense electronic energy deposition along high-energy ion trajectory.

Keywords: *Coupled model; Irradiation effect; Order to disorder phase transformation; Microstructure formation mechanism*

1. Introduction

Lithium niobate ($LiNbO_3$) crystal, as one of the most attractive ferroelectric functional materials due to its outstanding acousto-optic, electro-optic and nonlinear properties, has been widely used in the optical communication, laser technique and other optics applications. In the past several decades, much of research attentions have been carried out to understand the performance evolution of $LiNbO_3$ crystal in an irradiation environment and applications of property modification by ion irradiation in this material [1-4]. So far, the physical mechanism of the irradiation damage induced by the nuclear energy loss due to elastic collisions between energetic ions and target nuclei has been well understood [5-8], and recent studies have also revealed that $LiNbO_3$ crystal is very sensitive to ionizing irradiation and can be readily damaged due to electronic excitation primarily produced by inelastic collisions between ions and target electrons, which could be reasonably explained utilizing the thermal spike model [8-11] or models based on the accumulation of radiation-induced point defects (defect-assisted phase transition) [12-18]. Moreover, ion-beam-induced plastic deformation (atomic rearrangement provoked by electronic excitation and ionization) has been found in completely-disordered metallic glasses, but not crystalline metals [19,20], which reveals that the material in its amorphous phase would be more sensitive to the electronic energy loss than in its crystalline phase. Based on a recent publication in crystalline metal and complex alloys with distorted lattice [21], the possible impact from energy dissipation to defect evolution has been reported. Their findings show that changes in altered energy dissipation have a profound impact on defect dynamics, suggesting a direct correlation to radiation resistance. While energy dissipation pathway can be altered by compositional complex [21],

the more localized heat can also be achieved from the existence of the disorders. Therefore, under nuclear energy deposition, the sensitivity of materials to electronic energy loss could be enhanced due to the formation of displacement damage. Based on experimental results of low and high energy ion irradiations in recent years, intense electronic energy loss could induce either competitive or synergistic effects with the nuclear energy loss in some ceramic crystals and metallic materials: (a) electronic energy loss from high energy ion irradiation could induce epitaxial crystallization behavior at the amorphous/crystal interface, or damage annealing of the partly-damaged materials, as competitive effects represented by SiC [5,7,22-24], quartz [25], or some pure metals [20]; (b) defects produced by elastic collisions could greatly enhance intensity of thermal spike induced by intense electronic energy loss during high-energy ion irradiation, and therefore promote formation of amorphous tracks and significantly increase the damage production in the crystal, as synergistic effects represented by $SrTiO_3$ [26,27], InP or GaAs [28]. It is, therefore, fundamental to understand the correlation and interaction between the nuclear and electronic energy loss in $LiNbO_3$ crystal under ion irradiation.

Sequential irradiation of He and Fe ion with relative low energy has revealed the enhanced accumulation behavior of irradiation damage in $LiNbO_3$ crystal. However, this, ultimately, has been attributed to the formation of long-range strain/stress field coming from the irradiated He inclusions [29]. In view of all the above-mentioned irradiation effects, it should be quite attractive to study the damage behavior of $LiNbO_3$ crystal irradiated by ions with a wide energy range in order to further evaluate irradiation effect induced by non-correlated nuclear collisions and electronic excitations, and the possible competitive or synergistic effect

between these two kinds of interactions and the coupled irradiation phenomenon [6,7,30,31]. In this work, z-cut $LiNbO_3$ crystal with (0001) surface normal zone axis direction was irradiated at room temperature (300 K) with low (0.9 MeV Si^+) and high (21 MeV Si^{7+}) energy Si ions separately and also sequentially. Based on the Rutherford backscattering spectrometry (RBS) and channeling technique, the main purpose of this work is to better understand the damage evolution behavior of $LiNbO_3$ crystal resulting from different ion energy deposition processes: with the ion energy of 0.9 MeV and 21 MeV, with variables of nuclear and electronic energy loss, and ion fluence.

2. Simulation and experiment details

2.1. SRIM simulation

As shown in Fig. 1(a), the nuclear and electronic energy loss profile induced by 0.9 MeV Si^+ or 21 MeV Si^{7+} ions in $LiNbO_3$ are determined through SRIM 2012 full-cascade simulation code [32,33], in which the density of 4.65 g cm^{-3} and threshold displacement energies of 25 eV for Li, 25 eV for Nb and 28 eV for O sublattices were used [34]. The SRIM-predicted damage profile is determined from the sum of the predicted Li, Nb and O vacancy concentrations and the replacement events. Under 0.9 MeV Si^+ irradiation, the calculated conversion factor at damage peak (~ 650 nm) from ion fluence (10^{14} cm^{-2}) to dose in displacements per atom (dpa) is 0.054 at an incident angle 7° off the surface normal to avoid channeling effects. At the damage peak (~ 650 nm) of 0.9 MeV Si^+ (0.03 MeV/amu) irradiation, the electronic energy loss is ~ 0.7 keV/nm and the nuclear energy loss is ~ 0.24 keV/nm, which indicates that the ratio of electronic to nuclear energy loss (S_e/S_n) for 0.9 MeV Si^+ would drop as low as 3. In the near surface region (0 – 1 μm depth) under 21 MeV

Si^{7+} (0.75 MeV/amu) irradiation, the electronic energy loss reaches a saturation level (5.8 keV/nm, around the Bragg peak) and the nuclear energy loss is ~ 0.0073 keV/nm, which indicates that the ratio of electronic to nuclear energy loss (S_e/S_n) for 21 MeV Si^{7+} would rise as high as 795. Si ions with 0.9 MeV and 21 MeV were chosen in our work, as the representative of the low- and high-energy ions, respectively, to study the damage evolution behavior of $LiNbO_3$ induced by the nuclear and electronic energy loss in an ion irradiation environment.

2.2. Irradiation and RBS/C analysis

The ion irradiation process and the subsequent study of the damage evolution based on the ion channeling method were carried out using the 3.0 MV tandem accelerator facility (9SDH-2) within the UT-ORNL (University of Tennessee - Oak Ridge National Laboratory) Ion Beam Materials Laboratory (IBML) located on the UT campus [35]. Experimentally, z-cut $LiNbO_3$ crystal samples with (0001) surface normal zone axis direction used in this study were cut from a surface acoustic wave (SAW) grade $LiNbO_3$ crystal wafer of Φ 76.2 mm × 0.5 mm obtained from MTI Corporation [36]. These samples were coated with a carbon foil of ~ 10 nm to minimize charge accumulation on sample surface during ion irradiation and ion beam analysis. The Si-ion irradiation was performed at 300 K and during this process, the ion beam was rastered over the irradiation area with fixed horizontal and vertical scan frequencies to ensure uniform irradiations. In the Rutherford backscattering/channeling (RBS/C) analysis [35], 3.5 MeV He^+ beam with the flux of 8.3 × 10^{12} cm^{-2} s^{-1} extracted from the accelerator was used to determine the Si-induced damage in $LiNbO_3$ samples with the probe size of 1.5 × 1.5 mm^2. A Si detector located at a scattering

angle of 155° relative to the incoming beam was used to collect the signal of the backscattered He^+ yield from the pristine and irradiated $LiNbO_3$ samples. Through rotating the sample holder, the main axial channeling orientation and He beam can be aligned, which corresponds to the minimum He^+ yield.

There are three sets of irradiation and related RBS/C analysis. (i) For the first sample, it was irradiated at 7° off the channeling direction by 0.9 MeV Si^+ with a beam flux of 1.04×10^{12} cm^{-2} s^{-1} to an ion dose ranging from ~ 0.1 to ~ 1.4 dpa at the damage peak. The size of each irradiated area with different fluence was 3×3 mm^2. Subsequently, 3.5 MeV He^+ beam was utilized to carry out RBS/C analysis on these Si^+-irradiated regions to determine the disorder profile of $LiNbO_3$ produced from the low-energy Si ion irradiation to different fluences. As shown in Fig. 1(b), the regions of Si^+ irradiation and He^+ analysis are clearly displayed in the sample. (ii) For the second sample, it was irradiated both along and at 7° off the channeling direction by 21 MeV Si^{7+} with the beam flux of 2.48×10^{10} cm^{-2} s^{-1} to an ion fluence ranging from 5×10^{11} cm^{-2} to 2×10^{13} cm^{-2}, and the size of each irradiation area was also 3×3 mm^2. 3.5 MeV He^+ beam was then extracted to perform RBS/C measurements on these Si^{7+}-irradiated regions to analyze the damage behavior of $LiNbO_3$ under the high-energy ion irradiation along or at 7° off the <0001> channeling direction. (iii) For the third sample, firstly, two regions with the size of 8×8 mm^2 were irradiated by 0.9 MeV Si^+ with two different fluences, respectively, to produce two different initial disorder levels. The initial damage level was then evaluated by RBS/C using 3.5 MeV He^+ beam. With known pre-damage levels, these two Si^+-irradiated regions were irradiated with 21 MeV Si^{7+} ions along <0001> direction with the fluence ranging from 5×10^{11} cm^{-2} to 2×10^{13} cm^{-2},

respectively. Each irradiated area with different fluence was also 3 × 3 mm^2. The 3.5 MeV He^+ beam was extracted again to perform RBS/C measurements on these areas to analyze damage evolution of $LiNbO_3$ under the additional 21 MeV Si^{7+} irradiation.

3. Results and discussion of respective 0.9 MeV Si^+ or 21 MeV Si^{7+} irradiation

During ion irradiation process, an energetic Si ion will interact with both target nuclei and electrons and lose its energy via two processes: (i) nuclear (elastic) energy deposition induced by elastic collision, which could create a cascade of atomic collision events, displace the atoms from their initial sites (characterized by the nuclear energy loss shown in Fig. 1(a)) and finally produce permanent atomic-scale defects in the $LiNbO_3$ crystal structure; and (ii) electronic (inelastic) energy deposition (characterized by the electronic energy loss shown in Fig. 1(a)), which could induce ionization and electronic excitation. Based on the thermal spike model [37], the electronic energy loss from incident Si ions transferred to the target electrons results in electron cascade due to fast electron-electron interactions. Such energy is then transferred to $LiNbO_3$ lattice through electron-phonon interactions, which will lead to a temperature rise along the ion trajectory. Once the value of the electronic energy loss is above a certain threshold, local melt becomes possible. Tracks containing partially or completely amorphous volume could be formed during the rapid cooling phase. The former elastic collisions from the nuclear energy deposition is the dominate contribution during low energy ion (such as 0.9 MeV Si^+, 0.03 MeV/amu) irradiation process, and the latter ionization effects will become more obvious once the ion energy is high enough (such as 21 MeV Si^{7+}, 0.75 MeV/amu), both of which could significantly change the physical and chemical properties of $LiNbO_3$ crystal under irradiation conditions. In this work, the damage evolution behavior of

z-cut $LiNbO_3$ crystal irradiated using Si-ions with different energies will be discussed in detail.

3.1. 0.9 MeV (low energy) Si^+ irradiation

3.1.1. RBS results and damage analysis

The measured RBS/C spectra of z-cut $LiNbO_3$ crystal irradiated by 0.9 MeV Si^+ are shown in Fig. 2(a), which clearly illustrate the surface edges for Nb and O sublattices, and the non-Rutherford backscattering peak from O sublattices (interact with 3370 keV He) [38]. Utilizing an iterative procedure to analyze each RBS/C spectrum and determine the dechanneling component accurately [39], direct backscattering contribution from displaced atoms at each corresponding channel number could be calculated and therefore the disorder distributions of Nb sublattices as a function of the channel number could be further determined. After converting the channel number to depth in nanometers based on the energy difference at each channel and He-ion electronic energy loss in $LiNbO_3$ from SRIM 2012 simulation [32,33], the relative Nb-disorder as a function of depth could be obtained and shown in Fig. 2(b). Two obvious features should be pointed out: depth shift and enhanced surface damage.

The depth shift of the damage peak position is evident. In the case of the minimum dose (0.054 dpa at damage peak), the damage peak is located at 623 nm, which is shallower than that of SRIM 2012 simulation (650 nm), and while the damage increases with the irradiation dose, the peak position moves progressively to the surface. This phenomenon could be attributed to two factors: (i) sputtering effect of low-energy Si ion irradiations. As shown in Fig. 1(b) from the color change, the deposited carbon conducting film has been obviously

sputtered by the irradiated Si ions, which could indicate the non-negligible sputtering effects. The actual sputtering rate depends on surface conditions and irradiation conditions. Based on SRIM 2012 simulation, the sputtering yield for $LiNbO_3$ irradiated by 0.9 MeV Si^+ should be approximate 1 atom/ion, which means that the sputtering effect couldn't lead to the obvious depth shift on its own and it is only part of the reason for the depth shift. It is worth noting that SRIM prediction may have a large uncertainty based it generic input parameters. (ii) evolution of irradiation defect and microstructure, which is the main reason and has been observed in $SrTiO_3$ [39] and some other ceramics. The damage peak position may partly depend on the backscattering possibility of He-ion versus the defect types under different irradiation doses. Irradiation-induced interstitials and small amorphous clusters will cause direct backscatter and be detected easily compared to the vacancies or dislocation loops, which mainly increase the dechanneling yield, and this process will affect the energy of backscattered He-ion and be responsible for the depth shift of the damage peak.

The second noticeable feature is surface damage induced by electronic energy loss. As the fluence of irradiated Si^+ ion increases to 5×10^{14} cm^{-2} (0.27 dpa at damage peak), the surface damage of $LiNbO_3$ crystal will increase visibly, which, in addition to possible complex surface effects, is in fact a clear evidence of the cumulative behavior of the electronic energy loss (1.4 keV/nm, shown in Fig. 1(a)) of 0.9 MeV Si^+ on the sample surface. In reference [10], an improved thermal-spike model has been proposed to illuminate the damage formation in $LiNbO_3$ based on the latent track generated by MeV ion irradiation through electron excitation mechanism. In this model, although the electronic energy loss of each single irradiated-ion couldn't reach the threshold value for lattice amorphization, halo and tail

regions surrounding single ion path still could be formed and these regions produced by each ion will overlap with each other as a consequence of the cumulative contribution of ion fluence [13-15]. Once the formation and accumulation of point defects overcome a critical concentration, defect-assisted phase transition will happen [12], and the highly disordered region will therefore collapse, which thickness will increase and move to the interior of the material. This can explain the "U"-shape of the damage profile located at ~ 100 nm and the related evolution behavior with increasing the fluence, as shown in Fig. 2(b). The observed surface damage behavior of $LiNbO_3$ shown in Fig. 2(a) and (b) clearly concludes that due to the electronic energy loss exhibits a clear synergistic (additive) behavior, low electronic energy loss during MeV ion irradiation could also induce irradiation damage in $LiNbO_3$ crystal once the ion fluence increases to a certain value.

3.1.2. Damage accumulation produced from nuclear collision

The accumulated disorder at the buried damage peak for the Nb sublattices is shown in Fig. 2(c) as a function of local dose (dpa) for $LiNbO_3$ irradiated by 0.9 MeV Si^+ at 300 K. The damage accumulation produced from elastic collisions between the low-energy ions and target nuclei can be described by a disorder accumulation model [40-42], in which the total relative disorder, S, produced under ion beam irradiation and measured by ion-channeling method, could be given by the expression:

$$S = f_a + S_d + S_c \quad (1)$$

where f_a is the irradiation-induced amorphous fraction, and S_d is the relative disorder from the irradiation-induced interstitials and small interstitial clusters in the residual crystalline regions. S_c accounts for the relative disorder from the evolution of extended defect clusters,

which may provide significant contributions to the disorder at higher irradiation temperature, where point defects are more mobile and in the case of the irradiation at 300 K in this study, the contribution of S_c to the total disorder is insignificant and could be negligible. The amorphous fraction f_a is described using a direct-impact/defect-stimulated (DI/DS) model [43], where amorphization occurs directly within a cascade and from defect-stimulated processes at crystalline/amorphous interfaces, and could be given by the expression:

$$f_a = 1 - (\sigma_a + \sigma_s)/\{\sigma_s + \sigma_a exp[\sigma_a + \sigma_s]D\} \quad (2)$$

where σ_a is the amorphization cross section, σ_s is the effective cross section for defect-stimulated amorphization, and D is the local dose (dpa). The disorder from irradiation-induced interstitials and small interstitial clusters is described by a simple defect accumulation model and could be given by the expression:

$$S_d = S_d^*[1 - exp(-BD)](1 - f_a) \quad (3)$$

where S_d^* is the saturation value for the defect-induced disorder, and B (dpa^{-1}) is proportional to an effective recombination volume for the specific defects giving rise to S_d. As shown in Fig. 2(c), based on the disorder accumulation model, the solid, dash and dot curves, representing the S, f_a and S_d, respectively, are the fits to the experimental data and the corresponding fitting parameters are summarized in the figure. The relative disorder (S_d) from the irradiation-induced interstitials and small interstitial clusters holds a predominant contribution in the case of low irradiation dose, and the contribution (f_a) from the defect-stimulated amorphization process becomes significant with the irradiation dose. Since the crystalline fraction (1-f_a) decreases as a result of the increasing amorphous fraction (f_a), the contribution from the defect disorder (S_d) eventually reduces. The fitted damage

accumulation curve in this work is consistent with that obtained utilizing 0.35 MeV Ar^+ irradiation at 300 K in the reference [34] due to the similar mass number and energy of the irradiated Si and Ar ions. Utilization of the sigmoidal dependence of damage accumulation on irradiation dose could provide better understanding of the damage evolution behavior of $LiNbO_3$ crystal induced by the nuclear energy loss in the low-energy ion radiation environment.

3.2. 21 MeV (high energy) Si^{7+} irradiation

3.2.1. RBS results and damage analysis

The measured RBS/C spectra of z-cut $LiNbO_3$ crystal irradiated by 21 MeV Si^{7+} both along and at 7° off the channeling direction are shown in Fig. 3(a) and the related Si^{7+} ion fluences are also indicated. Owing to the rather thick damage layer induced by 21 MeV Si^{7+} irradiation, the damage at the maximum depth detected by 3.5 MeV He^+ beam does not fall to zero, and therefore the iterative procedure using in Section *3.1.1.* is inadaptable to determine the dechanneling component in this case. However, due to the dechanneling yield on the surface channel (1500 channel, which is just lower than the channel of Nb surface peak) is relatively low and can therefore be ignored (surface approximation) [44,45], the relative disorder fraction f_d in the surface region corresponding to the channel number of 1500 could be calculated through a classical approximate expression:

$$f_d = (\chi_i - \chi_v)/(\chi_r - \chi_v), \quad (4)$$

where χ_i, χ_v and χ_r are the backscattering yields of the irradiated sample in channeling condition, the virgin sample along <0001> channeling direction and in a random orientation, respectively.

In this case, based on SRIM 2012 simulation shown in Fig. 1(a), the dpa and damage at $LiNbO_3$ surface induced by the nuclear energy loss of Si^{7+} ion would be extremely low, and therefore the increase of the backscattering He^+ yield should be attributed to the electronic energy loss (5.8 keV/nm, at the surface) from 21 MeV Si^{7+} (0.75 MeV/amu), which is just around the threshold value (~ 5-6 keV/nm) required for the formation of the homogeneous amorphous layers in Si- and F-irradiated $LiNbO_3$ [15,46]. The RBS/C spectra of 21 MeV Si^{7+} irradiation with the fluence of 2×10^{13} cm^{-2} along the channeling direction is further discussed to understand the damage behavior of $LiNbO_3$ induced by the high electronic excitation. As shown in Fig. 3(b), the backscattering yield of the irradiated $LiNbO_3$ in channeling condition at the depth of 820 nm has reached to the random level, which means that compared to the damage level of ~ 81% at the surface ($f_{d,sur}$, 1500 channel), the corresponding damage level at the depth of 820 nm ($f_{d,dep}$) will increase to 100%. One reason of this state could be partially attributed to the surface effect, which means that the surface can serve as defect sink to anneal defects and decrease the damage level. Meanwhile, the phenomenon of the irradiation-damage increase from the surface to the depth of 820 nm could also demonstrate the velocity dependence of the damage cross-section induced by the high electronic excitation [37,40]. The SRIM 2012 simulation shown in Fig. 1(a) has illustrated that in the near surface region, the electronic energy loss (S_e) of 21 MeV Si^{7+} in $LiNbO_3$ coincidentally situates around the Bragg peak, and therefore the S_e from surface to 1 μm deep should approximatively keep constant. While SRIM 2012 results could only be appropriate for the non-crystalline material, it would be still reasonable to consider that under the channeling irradiation, the S_e at the surface ($S_{e,sur}$) is approximatively equal to that at the

depth of 820 nm ($S_{e,dep}$). The energy deposition during ion penetration process will reduce the ion energy from 21 MeV (0.75 MeV/amu) at the surface (E_{sur}) to 16 MeV (0.57 MeV/amu) at the depth of 820 nm (E_{dep}), and the energy difference of 5 MeV (0.18 MeV/amu) could quantitatively represent the obvious decrease of the ion velocity from surface to the depth of 820 nm. In the case of the same S_e, the decrease of ion velocity will lead the effective radius of ion track produced by S_e at the depth of 820 nm larger than that at the surface, and therefore the corresponding irradiation damage at the depth of 820 nm will be more significant ($f_{d,dep} > f_{d,sur}$), which could reasonably explain the trend of the other RBS/C spectra of $LiNbO_3$ irradiated by the high energy Si^{7+} ions, as shown in Fig. 3(a).

3.2.2. Damage accumulation produced from electronic excitation

The evolution of Nb-disorder fraction f_d at the surface corresponding to channel number of 1500 versus the irradiation fluence Φ has been presented in Fig. 3(c), and the solid lines are the best fit obtained with Avrami curve [16]:

$$f_d = 1 - \exp\{-(\Phi/\Phi_0)^n\}, \quad (5)$$

where the parameters n and Φ_0 strongly depend on the electronic energy loss (S_e). The observation of the Avrami-like (sigmoidal) kinetics shows clear evidence of the cumulative behavior of the irradiation damage due to electronic excitation [15]. Moreover, since ions along channeling direction have lower probability of a close encounter with atom rows and therefore have reduced the interactions with inner-shell electrons of target atoms, the channeled ions usually have a stopping power lower than that of random ions [47,48,49]. Consequently, less damage will be created along a channeling direction than 7°-off-channeling irradiation, which is also clearly evident through the RBS/C spectra shown

in Fig. 3(c). For instance, under 21 MeV Si^{7+} (0.75 MeV/amu) irradiation with the fluence of 2×10^{13} cm^{-2}, the surface of $LiNbO_3$ coincidentally becomes amorphous under non-channeling ion irradiation, and once the irradiation is carried out along the channeling direction, the damage level will decrease to ~ 81% due to the reduced electronic energy loss of channeled ions.

4. Results and discussion of sequential 0.9 MeV Si^+ and 21 MeV Si^{7+} irradiation

As mentioned in Section *3.*, the nuclear and electronic energy loss would become the dominating element during the low and high energy ion irradiation, respectively. In order to understand the coupled or combined effects of the nuclear and electronic energy loss, the low and high energy ion irradiations have been developed to evaluate their effects [5,26,50,51]. These results have indicated that, for some particular crystals (SiC, $SrTiO_3$, etc) or pure metals, the subsequent electronic energy loss could anneal the pre-existing damage or significantly enhance damage production, both of which could be explained by a thermal spike mechanism. In our work, the sequential ion irradiation experiment has also been carried out to study the damage evolution of pre-damaged $LiNbO_3$ irradiated by high energy ions and therefore to evaluate the competitive or synergistic effect between the nuclear and electronic energy loss. Two pre-damaged regions in $LiNbO_3$ crystal with Nb-disorder of 0.23 and 0.6 at damage peak, respectively, are produced utilizing 0.9 MeV Si^+ ion irradiation, and subsequently irradiated by 21 MeV Si^{7+} to different fluences along the channeling direction.

4.1. Sequential 0.9 MeV (low energy) Si^+ and 21 MeV (high energy) Si^{7+} irradiation

4.1.1. RBS results and damage analysis

As shown in Fig. 4, the measured RBS/C spectra clearly indicate that the damage level of the

pre-damaged $LiNbO_3$ will progressively increase accompanied with the increasing Si^{7+} ion fluence. The results indicate that in the pre-damaged $LiNbO_3$, the intense electronic energy loss during the high energy ion (21 MeV Si^{7+}) irradiation will continue to produce damage, but not the swift heavy ion beam induced epitaxial crystallization (SHIBIEC) effect.

Additionally, to study the effect of the pre-existing defect on the damage behavior induced by inelastic electronic energy loss, the Nb-disorder $(f_{d,n}\ \&\ f_{d,e})$ corresponding to the channel number of 1500 in this case has been calculated from the RBS/C spectra shown in Fig. 4 utilizing the classical approximate expression in Section *3.2.1.*, and the sum of the Nb-disorders $(f_{d,n} + f_{d,e})$ induced independently by the low energy Si^+ and high energy Si^{7+} irradiations, respectively, has also been calculated based on the results shown in Fig. 2 and Fig. 3. As shown in Fig. 5(a) and (b), no matter what the initial damage at the damage peak is ($f_{d,e}$: 0.06 or 0.24), both the values of $(f_{d,n}\ \&\ f_{d,e})$ minus $(f_{d,n} + f_{d,e})$ are positive and show the similar evolution rule considering the change trend of the red and blue lines: firstly, the damage increment will increase with the increasing ion fluence. Once the ion fluence increases to a certain value, the damage increment will then decrease with the increasing ion fluence. Figure 5 clearly indicates that compared to the damage in pristine crystal solely induced by electronic energy loss, the pre-existing defects produced by nuclear collisions could act as damage seeds, and obviously promote damage formation and further increase damage level induced by electronic energy loss.

If a single ion results in a continuous amorphous track, the increase in the fraction of amorphous phase, f_d, with increasing ion fluence, Φ, could be given by the direct or single impact model [26,43,52]:

$$f_d = 1 - \exp(-\sigma_a \Phi) \quad (6)$$

where σ_a is the amorphous cross-section of the track. Due to the pre-existing disorder or damage in the sample prior to irradiation with 21 MeV Si^{7+}, equation (6) is modified to take into account the local pre-existing disorder, f_0. This modified direct impact model is given by:

$$f_d = f_0 + (1 - f_0)[1 - \exp(-\sigma_a \Phi)] \quad (7)$$

The track radius, r, could be readily obtained from the relationship:

$$\sigma_a = \pi r^2 \quad (8)$$

Equations (7) and (8) could be used to quantitatively calculate the damage cross-section σ_a and the radius r of the ion track produced by Si^{7+} irradiation in pristine or pre-damaged $LiNbO_3$ based on the measured Nb-disorder level. In order to rule out the effect of the dechanneling yield on Nb-disorder, we still only consider the damage at $LiNbO_3$ surface (channel number: 1500) in the analysis process. The related initial Nb-disorder f_0 at the surface corresponding to two pre-damaged regions in $LiNbO_3$ is 0.060 and 0.244, respectively, and for pristine $LiNbO_3$, f_0 should be equal to zero. When the ion fluence increases to 5×10^{12} cm^{-2}, the induced ion track will overlap with each other and further affect our calculation, so only the fluence of 5×10^{11} cm^{-2} and 2×10^{12} cm^{-2} would be analyzed and in this case, the ion track should be isolated. Finally the calculated damage cross-section σ_a and the radius r of ion track corresponding to the above parameters are summarized in Table 1, which clearly shows the evidence of the obvious increase of σ_a and r induced by 21 MeV Si^{7+} irradiation in pre-damaged $LiNbO_3$ ($f_0 = 0.060, 0.244$) compared to pristine $LiNbO_3$ ($f_0 = 0$). Our results indicate that σ_a and r of ion track induced by the

high electronic energy loss directly depend on the initial damage level f_0.

4.1.2. Coupled effect between nuclear energy loss and electronic energy loss

We used an inelastic thermal spike (iTS) model [53] suitable for insulators to include the electronic energy loss effects in the simulations. In this model, the atomic and the electronic subsystems are coupled and the energy exchange between them is described via a set of heat diffusion equations: one describing the evolution of the electronic temperature, T_e, as given by equation (9), and one describing the evolution of the atomic temperature, T_a, as given by equation (10).

$$C_e(T_e)\frac{\partial T_e}{\partial t} = \frac{1}{r}\frac{\partial}{\partial r}\left[rK_e(T_e)\frac{\partial T_e}{\partial r}\right] - g(T_e - T_a) + A(r,t) \quad (9)$$

$$C_a(T_a)\frac{\partial T_a}{\partial t} = \frac{1}{r}\frac{\partial}{\partial r}\left[rK_a(T_a)\frac{\partial T_a}{\partial r}\right] + g(T_e - T_a) \quad (10)$$

The hot electrons transfer energy to the lattice via the electron-phonon interactions. The second term on the right side of the equations (5) and (6) represents the energy exchange between the electronic and atomic subsystems due to the difference between T_e and T_a. The parameters C_e and C_a are the specific heat coefficients of the electronic and atomic systems, respectively; whereas, K_e and K_a are the thermal conductivities of the electronic and the atomic systems, respectively. The term g is the electron-phonon coupling parameter, and $A(r,t)$ describes the energy deposition from the incident ion to the electrons [54].

Compared to the crystalline system, irradiation-induced defects in the pre-damaged system are known to (i) scatter phonons and electrons resulting in significant decrease in the thermal conductivity (K_e and K_a) of irradiated ceramics [55,56], and (ii) decrease the electron-phonon mean free path resulting in obvious increase in the electron-phonon coupling parameter g. Based on the iTS model, the fundamental mechanism causing the damage

behavior in Section *4.1.1.* could be ascribed to the reduced electronic and atomic thermal conductivities, K_e and K_a, and the increased electron-phonon coupling parameter g due to the pre-existing defect formation in the crystal. This physical process could enhance the sensitivity of crystal to the effect of electronic energy loss and increase the temperature at the thermal spike core during each high energy ion penetration process [26]. In addition, the observed enhance of the disorder level can be also understood as a clear consequence of decreasing the electronic amorphization threshold because of a pre-existing highly disordered region produced by nuclear energy loss in well agreement with the cumulative models [57]. These results demonstrate that the nuclear energy loss could interact synergistically with the electronic energy loss to promote the formation of the amorphous track, increase the track diameter with depth and produce more significant irradiation-induced damage region. To have the capability of controlling the amorphous ion track radii in depth (ion track profiles) based on the coupled effect of electronic and nuclear energy loss turns into a very promising tool to perform tailored modification of optical properties (refractive index profiles) of the irradiated material to be exploited in future devices for novel photonic applications [11,58]. Optimizing the irradiation parameters (ion, energy, fluence, angle of irradiation) will produce an accurate control of the optical properties of the modified material.

5. Conclusions

Employing 0.9 MeV Si^{+} and 21 MeV Si^{7+} as the representative of low and high energy ions to deposit significant nuclear and electronic energy, respectively, damage evolution behavior of z-cut $LiNbO_3$ crystal in different ion irradiation environments has been studied at 300 K using RBS/C technique. For 0.9 MeV Si^{+}, damage accumulation in $LiNbO_3$ crystal has been

investigated and damage produced by low electronic energy loss have been confirmed. For 21 MeV Si^{7+}, damage level in the surface region as a function of ion fluence has been analyzed. The increase of the damage from the surface to a deeper depth demonstrates the velocity dependent effect on damage cross-section induced by high electronic excitation. What's more remarkable is the observable nonlinear additivity of irradiation damage induced by the electronic energy loss in partly-damaged $LiNbO_3$ crystal. Defects produced by elastic collisions could enhance temperature of the thermal spike core resulting from intense electronic energy loss, which concludes that defects resulting from nuclear energy loss could interact synergistically with inelastic electronic energy deposition. The coupled synergistic effect could be used to promote formation of amorphous tracks, to increase track diameter, or to significantly enhance damage evolution, compared to damage in pristine crystal solely produced by electronic energy loss during the high energy ion irradiation. An accurate control of ion track profiles based on the coupled effect during ion beam irradiation turns into a very promising tool to perform tailored refractive index profiles to be exploited in future devices for novel photonic applications.

Acknowledgements

The work was supported by the U.S. Department of Energy, Office of Science, Basic Energy Sciences, Materials Science and Engineering Division. P. Liu was supported by the China Scholarship Council (CSC) overseas scholarship program during his visit at UTK and by the National Natural Science Foundation of China (Grant No. 11405097) and the Natural Science Foundation of Shandong Province of China (Grant No. ZR2014AQ021). All the experiments were performed at the UT-ORNL ion beam Materials Laboratory (http://ibml.utk.edu/).

References:

[1] P.D. Townsend, P. Chandler, L. Zhang, Optical effects of ion implantation, Cambridge University Press, 2006.

[2] G. Destefanis, J. Gailliard, E. Ligeon, S. Valette, B. Farmery, P. Townsend, A. Perez, The formation of waveguides and modulators in $LiNbO_3$ by ion implantation, J. Appl. Phys. 50 (1979) 7898.

[3] A. García-Navarro, F. Agulló-López, M. Bianconi, J. Olivares, G. García, Kinetics of ion-beam damage in lithium niobate, J. Appl. Phys. 101 (2007) 083506.

[4] G.G. Bentini, M. Bianconi, L. Correra, M. Chiarini, P. Mazzoldi, C. Sada, N. Argiolas, M. Bazzan, R. Guzzi, Damage effects produced in the near-surface region of x-cut $LiNbO_3$ by low dose, high energy implantation of nitrogen, oxygen, and fluorine ions, J. Appl. Phys. 96 (2004) 242.

[5] Y. Zhang, R. Sachan, O.H. Pakarinen, M.F. Chisholm, P. Liu, H. Xue, W.J. Weber, Ionization-induced annealing of pre-existing defects in silicon carbide, Nat. Commun. 6 (2015) 8049.

[6] L. Thomé, A. Debelle, F. Garrido, S. Mylonas, B. Décamps, C. Bachelet, G. Sattonnay, S. Moll, S. Pellegrino, S. Miro, P. Trocellier, Y. Serruys, G. Velisa, C. Grygiel, I. Monnet, M. Toulemonde, P. Simon, J. Jagielski, I. Jozwik-Biala, L. Nowicki, M. Behar, W.J. Weber, Y. Zhang, M. Backman, K. Nordlund, F. Djurabekova, Radiation effects in nuclear materials: Role of nuclear and electronic energy losses and their synergy, Nucl. Instrum. Methods Phys. Res., Sect. B 307 (2013) 43-48.

[7] Y. Zhang, T. Varga, M. Ishimaru, P.D. Edmondson, H. Xue, P. Liu, S. Moll, F. Namavar, C. Hardiman, S. Shannon, W.J. Weber, Competing effects of electronic and nuclear energy loss on microstructural evolution in ionic-covalent materials, Nucl. Instrum. Methods Phys. Res., Sect. B 327 (2014) 33-43.

[8] R. Sachan, O.H. Pakarinen, P. Liu, M.K. Patel, M.F. Chisholm, Y. Zhang, X.L. Wang, W.J. Weber, Structure and band gap determination of irradiation-induced amorphous nano-channels in $LiNbO_3$, J. Appl. Phys. 117 (2015) 135902.

[9] J. Olivares, G. Garcia, A. Garcia-Navarro, F. Agullo-Lopez, O. Caballero, A. Garcia-Cabanes, Generation of high-confinement step-like optical waveguides in $LiNbO_3$ by swift heavy ion-beam irradiation, Appl. Phys. Lett. 86 (2005) 183501.

[10] F. Agulló-López, G. García, J. Olivares, Lattice preamorphization by ion irradiation: Fluence dependence of the electronic stopping power threshold for amorphization, J. Appl. Phys. 97 (2005) 093514.

[11] J. Olivares, A. García-Navarro, G. García, A. Mendez, F. Agulló-López, Optical determination of three-dimensional nanotrack profiles generated by single swift-heavy ion impacts in lithium niobate, Appl. Phys. Lett. 89 (2006) 071923.

[12] H.J. Fecht, Defect-induced melting and solid-state amorphization, Nature 356 (1992) 133-135.

[13] A. Rivera, J. Olivares, M.L. Crespillo, G. García, M. Bianconi, F. Agulló-López, Assessment of swift-ion damage by RBS/C: Determination of the amorphization threshold, Nucl. Instrum. Methods Phys. Res., Sect. B 267 (2009) 1460-1463.

[14] A. Rivera, M.L. Crespillo, J. Olivares, G. García, F. Agulló-López, Effect of defect accumulation on ion-beam damage morphology by electronic excitation in lithium niobate: A MonteCarlo approach, Nucl. Instrum. Methods Phys. Res., Sect. B 268 (2010) 2249-2256.

[15] A. Rivera, J. Olivares, G. García, J.M. Cabrera, F. Agulló-Rueda, F. Agulló-López, Giant enhancement of material damage associated to electronic excitation during ion irradiation: The case of $LiNbO_3$, Phys. Status Solidi A 206 (6) (2009) 1109-1116.

[16] G. García, A. Rivera, M.L. Crespillo, N. Gordillo, J. Olivares, F. Agulló-López, Amorphization kinetics under swift heavy ion irradiation: A cumulative overlapping-track approach, Nucl. Instrum. Methods Phys. Res., Sect. B 269 (2011) 492-497.

[17] O. Caballero-Calero, A. García-Cabañes, M. Carrascosa, F. Agulló-López, J. Villarroel, M. Crespillo, J. Olivares, Periodic poling of optical waveguides produced by swift-heavy-ion irradiation in $LiNbO_3$, Appl. Phys. B 95 (2009) 435-439.

[18] J. Villarroel, M. Carrascosa, A. García-Cabañes, O. Caballero-Calero, M. Crespillo, J. Olivares, Photorefractive response and optical damage of $LiNbO_3$ optical waveguides produced by swift heavy ion irradiation, Appl. Phys. B 95 (2009) 429-433.

[19]. M.-D. Hou, S. Klaumünzer, G. Schumacher, Dimensional changes of metallic glasses during bombardment with fast heavy ions, Phys. Rev. B 41 (1990) 1144-1157.

[20]. A. Dunlop, D. Lesueur, P. Legrand, H. Dammak, J. Dural, Effects induced by high electronic excitations in pure metals: A detailed study in iron, Nucl. Instrum. Methods Phys. Res., Sect. B 90 (1994) 330-338.

[21] Y. Zhang, G.M. Stocks, K. Jin, C. Lu, H. Bei, B.C. Sales, L. Wang, L.K. Béland, R.E. Stoller, G.D. Samolyuk, M. Caro, A. Caro, W.J. Weber, Influence of chemical disorder on energy dissipation and defect evolution in concentrated solid solution alloys, Nat. Commun. 6 (2015) 8736.

[22] A. Debelle, M. Backman, L. Thomé, W.J. Weber, M. Toulemonde, S. Mylonas, A. Boulle, O.H. Pakarinen, N. Juslin, F. Djurabekova, K. Nordlund, F. Garrido, D. Chaussende,

Combined experimental and computational study of the recrystallization process induced by electronic interactions of swift heavy ions with silicon carbide crystals, Phys. Rev. B 86 (2012) 100102.

[23] M. Backman, M. Toulemonde, O.H. Pakarinen, N. Juslin, F. Djurabekova, K. Nordlund, A. Debelle, W.J. Weber, Molecular dynamics simulations of swift heavy ion induced defect recovery in SiC, Comp. Mater. Sci. 67 (2013) 261-265.

[24] A. Benyagoub, A. Audren, L. Thomé, F. Garrido, Athermal crystallization induced by electronic excitations in ion-irradiated silicon carbide, Appl. Phys. Lett. 89 (2006) 241914.

[25]. M. Toulemonde, S.M.M. Ramos, H. Bernas, C. Clerc, B. Canut, J. Chaumont, C. Trautmann, MeV gold irradiation induced damage in α-quartz: Competition between nuclear and electronic stopping, Nucl. Instrum. Methods Phys. Res., Sect. B 178 (2001) 331-336.

[26] W.J. Weber, E. Zarkadoula, O.H. Pakarinen, R. Sachan, M.F. Chisholm, P. Liu, H. Xue, K. Jin, Y. Zhang, Synergy of elastic and inelastic energy loss on ion track formation in $SrTiO_3$, Sci. Rep. 5 (2015) 7726.

[27] E. Zarkadoula, O.H. Pakarinen, H. Xue, Y. Zhang, W.J. Weber, Predictive modeling of synergistic effects in nanoscale ion track formation, Phys. Chem. Chem. Phys. 17 (2015) 22538-22542.

[28]. A. Kamarou, W. Wesch, E. Wendler, A. Undisz, M. Rettenmayr, Radiation damage formation in InP, InSb, GaAs, GaP, Ge, and Si due to fast ions, Phys. Rev. B 78 (2008) 054111.

[29]. H.-C. Huang, L. Zhang, G. Malladi, J.I. Dadap, S. Manandhar, K. Kisslinger, R.S. R Vemuri, V. Shutthanandan, H. Bakhru, R.M. Osgood, Radiation damage by light- and heavy-ion bombardment of single-crystal $LiNbO_3$, Opt. Mater. Express 5 (2015) 1071-1088.

[30] W.J. Weber, D.M. Duffy, L. Thomé, Y. Zhang, The role of electronic energy loss in ion beam modification of materials, Curr. Opin. Solid State Mater. 19 (2015) 1-11.

[31] M. Toulemonde, W.J. Weber, G. Li, V. Shutthanandan, P. Kluth, T. Yang, Y. Wang, Y. Zhang, Synergy of nuclear and electronic energy losses in ion-irradiation processes: The case of vitreous silicon dioxide, Phys. Rev. B 83 (2011) 054106.

[32] J.F. Ziegler, M.D. Ziegler, J.P. Biersack, SRIM – The stopping and range of ions in matter (2010), Nucl. Instrum. Methods Phys. Res., Sect. B, 268 (2010) 1818-1823.

[33] J.F. Ziegler, www.srim.org.

[34] F. Schrempel, T. Gischkat, H. Hartung, E.B. Kley, W. Wesch, A. Tünnermann, High

aspect ratio microstructures in $LiNbO_3$ produced by ion beam enhanced etching, Mater. Res. Soc. Symp. Proc. 908 (2005) 0908-OO16-01.

[35] Y. Zhang, M.L. Crespillo, H. Xue, K. Jin, C.H. Chen, C.L. Fontana, J.T. Graham, W.J. Weber, New ion beam materials laboratory for materials modification and irradiation effects research, Nucl. Instrum. Methods Phys. Res., Sect. B 338 (2014) 19-30.

[36] Website: www.mtixtl.com.

[37] A. Meftah, J.M.Costantini, N. Khalfaoui, S. Boudjadar, J.P. Stoquert, F. Studer, M. Toulemonde, Experimental determination of track cross-section in $Gd_3Ga_5O_{12}$ and comparison to the inelastic thermal spike model applied to several materials, Nucl. Instrum. Methods Phys. Res., Sect. B 237 (2005) 563-574.

[38] Y. Wang, M.A. Nastasi, Handbook of modern ion beam materials analysis, Materials Research Society, 2009.

[39] Y. Zhang, J. Lian, Z. Zhu, W.D. Bennett, L.V. Saraf, J.L. Rausch, C.A. Hendricks, R.C. Ewing, W.J. Weber, Response of strontium titanate to ion and electron irradiation, J. Nucl. Mater. 389 (2009) 303-310.

[40] Y. Zhang, F. Gao, W. Jiang, D.E. McCready, W.J. Weber, Damage accumulation and defect relaxation in 4H−SiC, Phys. Rev. B 70 (2004) 125203.

[41] Y. Zhang, W.J. Weber, W. Jiang, C.M. Wang, V. Shutthanandan, A. Hallen, Effects of implantation temperature on damage accumulation in Al-implanted 4H–SiC, J. Appl. Phys. 95 (2004) 4012.

[42] Y. Zhang, I.-T. Bae, W.J. Weber, Atomic collision and ionization effects in oxides, Nucl. Instrum. Methods Phys. Res., Sect. B 266 (2008) 2828-2833.

[43] W.J. Weber, Models and mechanisms of irradiation-induced amorphization in ceramics, Nucl. Instrum. Methods Phys. Res., Sect. B 166-167 (2000) 98-106.

[44] B. Canut, R. Brenier, A. Meftah, P. Moretti, S. Ould Salem, M. Pitaval, S.M.M. Ramos, P. Thevenard, M. Toulemonde, Latent track formation in $LiNbO_3$ single crystals irradiated by GeV uranium ions, Rad. Eff. and Defect in solids 136 (1995) 307-310.

[45] W.K. Chu, J.W. Mayer, M.A. Nicolet, Back-scattering Spectrometry, Academic Press, New York, 1978.

[46]. B. Caunt, S.M.M. Ramos, The concept of effective electronic stopping power for modelling the damage cross-section in refractory oxides irradiated by GeV ions or MeV clusters, Rad. Eff. and Defect in solids 145 (1998) 1-27.

[47]. M. Toulemonde, E. Balanzat, S. Bouffard, J.J. Grob, M. Hage-Ali, J.P. Stoquert, Damage induced by high electronic stopping power in SiO_2 quartz, Nucl. Instrum.

Methods Phys. Res., Sect. B 46 (1990) 64-68.

[48] F. Schrempel, T. Steinbach, T. Gischkat, W. Wesch, Channeling irradiation of $LiNbO_3$, Nucl. Instrum. Methods Phys. Res., Sect. B 266 (2008) 2958-2961.

[49]. J. Lindhard, Motion of swift charged particles, as influenced by strings of atoms in crystals, Phys. Lett. 12 (1964) 126-128.

[50] A. Meftah, F. Brisard, J.M. Costantini, M. Hage-Ali, J.P. Stoquert, F. Studer, M. Toulemonde, Swift heavy ions in magnetic insulators: A damage-cross-section velocity effect, Phys. Rev. B 48 (1993) 920-925.

[51] A. Benyagoub, A. Audren, Mechanism of the swift heavy ion induced epitaxial recrystallization in predamaged silicon carbide, J. Appl. Phys. 106 (2009) 083516.

[52] J.F. Gibbons, Ion implantation in semiconductors—Part II: Damage production and annealing, Proc. IEEE 60 (1972) 1062-1096.

[53]. M. Toulemonde, W. Assman, C. Dufour, A. Meftah, F. Studer, C. Trautmann, Experimental phenomena and thermal spike model description of ion tracks in amorphisable ionorganic insulators, Mat. Fys. Medd. K. Dan. Vidensk. Selsk. 52 (2006) 263-292.

[54]. M.P.R. Waligorski, R.N. Hamm, R. Katz, The radial distribution of dose around the path of a heavy ion in liquid water, Nucl. Tracks Radiat. Meas. 11 (1986) 309-319.

[55]. L.L. Snead, S.J. Zinkle, D.P. White, Thermal conductivity degradation of ceramic materials due to low temperature, low dose neutron irradiation, J. Nucl. Mater. 340 (2005) 187-202.

[56]. P.B. Weisensee, J.P. Feser, D.G. Cahill, Effect of ion irradiation on the thermal conductivity of UO_2 and U_3O_8 epitaxial layers, J. Nucl. Mater. 443 (2013) 212-217.

[57] F. Agullo-Lopez, A. Climent-Font, A. Munoz-Martin, J. Olivares, A. Zucchiatti, Ion beam modification of dielectric materials in the electronic excitation regime: cumulative and exciton models, Prog. Mater. Sci. 76 (2015) 1-58.

[58] J. Olivares, M.L. Crespillo, O. Caballero-Calero, M.D. Ynsa, A. García-Cabañes, M. Toulemonde, C. Trautmann, F. Agulló-López, Thick optical waveguides in lithium niobate induced by swift heavy ions (~10 MeV/amu) at ultralow fluences, Opt. Express 17 (2009) 24175-24182.

Table 1.

Experimental damage cross-section σ_a and radius r of ion track obtained from the direct impact model corresponding to $LiNbO_3$ surface (channel number: 1500)

Si^{7+} fluence (cm^{-2})	Track		Initial non-damage	Initial low-damage	Initial high-damage
Φ			$f_0 = 0$	$f_0 = 0.060$	$f_0 = 0.244$
			direct impact model:	$f_d = f_0 + (1 - f_0)[1 - \exp(-\sigma_a \Phi)]$, $\sigma_a = \pi r^2$	
			$f_d \approx 0$	$f_d = 0.106$	$f_d = 0.272$
5×10^{11}	isolated track	σ_a (nm^2)	~ 0	10.0	7.5
		r (nm)	~ 0	1.8	1.6
			$f_d = 0.014$	$f_d = 0.322$	$f_d = 0.518$
2×10^{12}	isolated track	σ_a (nm^2)	0.7	16.3	22.5
		r (nm)	0.5	2.3	2.7

Figure Captions:

Fig. 1. (a) The distributions of nuclear and electronic energy loss as a function of penetration depth for 0.9 MeV Si^{+} and 21 MeV Si^{7+} ions in $LiNbO_3$ based on SRIM 2012 simulation. (b) Partial image of 0.9 MeV Si^{+}-irradiated $LiNbO_3$ sample with carbon foil, which indicates the regions of Si^{+} irradiation and He^{+} analysis.

Fig. 2. (a) RBS/C spectra of $LiNbO_3$ irradiated by 0.9 MeV Si^{+} at 7° off channeling direction at 300 K. (b) Disorder profiles on Nb sublattice after irradiation to different ion fluence. (c) Relative disorder of Nb sublattice at the damage peak inside the crystal as a function of local dose. The lines are the fits of Eq. (1) to the data and the corresponding fit parameters are summarized in the inset.

Fig. 3. (a) RBS/C spectra of $LiNbO_3$ irradiated by 21 MeV Si^{7+} along or at 7° off channeling direction at 300 K. (b) RBS/C spectra of $LiNbO_3$ irradiated by Si^{7+} along channeling direction with the fluence of 2×10^{13} cm^{-2}, which shows the damage level at different ion penetration depth and confirms the velocity dependence of the damage cross-section. (c) Relative disorder of Nb sublattice at the surface as a function of local fluence. The solid lines are the best fit obtained with Avrami curve.

Fig. 4. RBS/C spectra of pre-damaged $LiNbO_3$ with Nb-disorder of 0.23 (a) and 0.6 (b) at damage peak irradiated by subsequent 21 MeV Si^{7+} along channeling direction to different ion fluence at 300 K.

Fig. 5. (a) The $(f_{d,n} \,\&\, f_{d,e})$ represents the Nb-disorder at $LiNbO_3$ surface corresponding to channel number of 1500 induced by the sequential low energy Si^{+} and high energy Si^{7+} irradiations, which is calculated from the RBS/C spectra shown in Fig. 4. The $(f_{d,n} + f_{d,e})$ means the sum of the Nb-disorders induced by the low energy Si^{+} and high energy Si^{7+} irradiations, respectively, which are based on the results shown in Fig. 2 and Fig. 3. (b) The difference of the Nb-disorder between $(f_{d,n} \,\&\, f_{d,e})$ and $(f_{d,n} + f_{d,e})$ clearly shows the damage increase during the sequential low energy Si^{+} and high energy Si^{7+} irradiations and demonstrates the synergistic effect between the nuclear energy loss during the low energy ion irradiation and the electronic energy loss during the high energy ion irradiation.

Fig. 1.

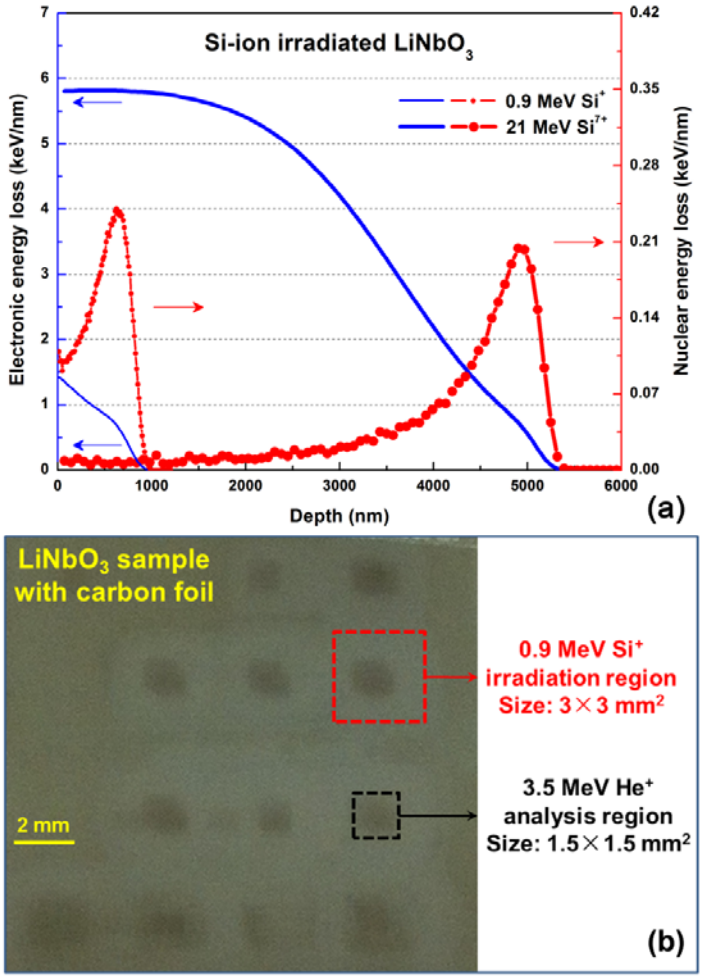
Si-ion irradiated LiNbO3
0.9 MeV Si+
21 MeV Si7+
Electronic energy loss (keV/nm)
Nuclear energy loss (keV/nm)
Depth (nm)
(a)
LiNbO3 sample
with carbon foil
0.9 MeV Si+
irradiation region
Size: 3×3 mm2
3.5 MeV He+
analysis region
Size: 1.5×1.5 mm2
2 mm
(b)

Fig. 2.

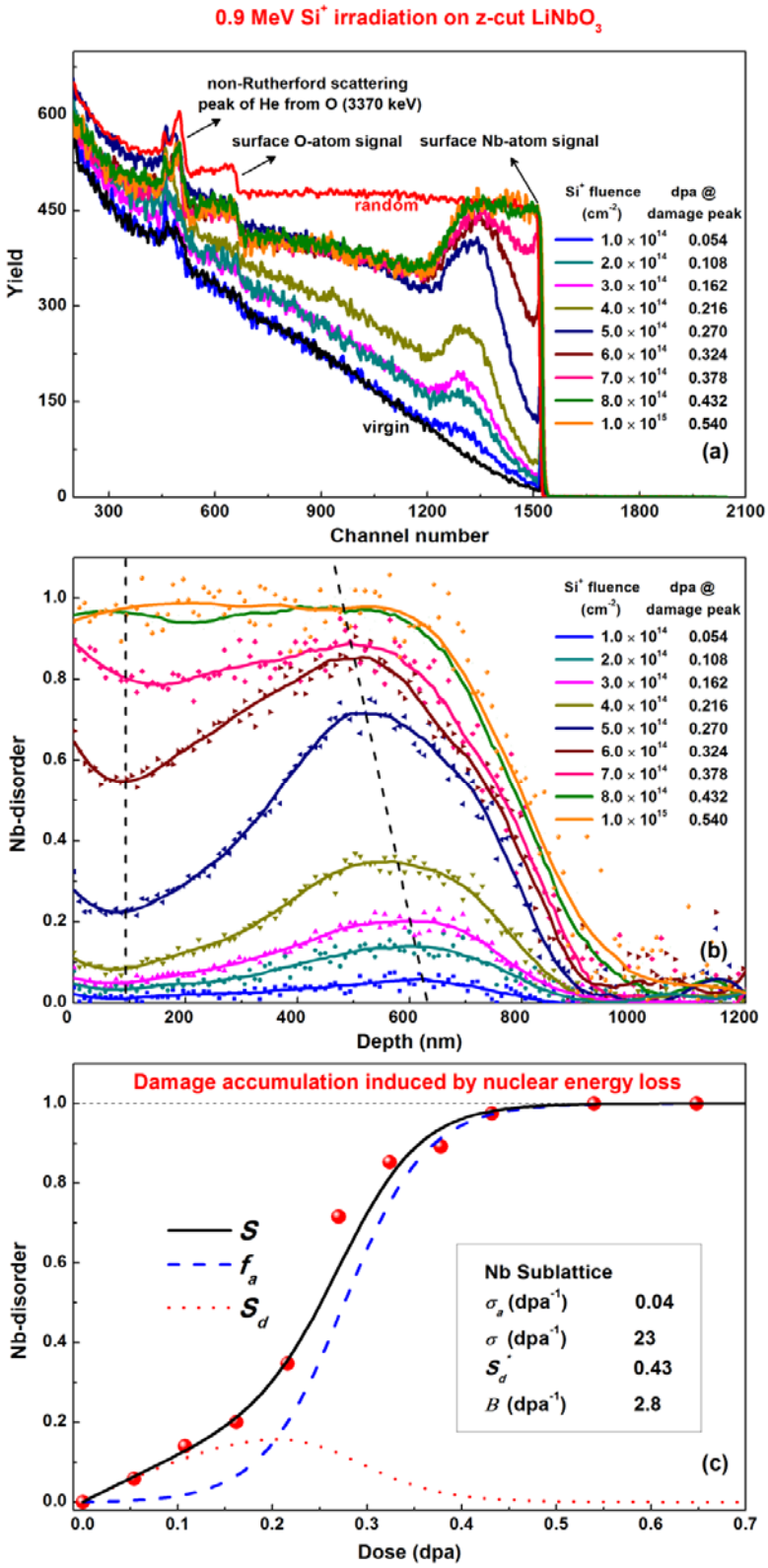
0.9 MeV Si+ irradiation on z-cut LiNbO3
non-Rutherford scattering
peak of He from O (3370 keV)
surface O-atom signal
surface Nb-atom signal
random
virgin
Yield
Channel number
Si+ fluence (cm-2)
dpa @ damage peak
1.0 × 10^14 0.054
2.0 × 10^14 0.108
3.0 × 10^14 0.162
4.0 × 10^14 0.216
5.0 × 10^14 0.270
6.0 × 10^14 0.324
7.0 × 10^14 0.378
8.0 × 10^14 0.432
1.0 × 10^15 0.540
(a)
Nb-disorder
Depth (nm)
(b)
Damage accumulation induced by nuclear energy loss
S
fa
Sd
Nb Sublattice
σa (dpa-1) 0.04
σ (dpa-1) 23
Sd* 0.43
B (dpa-1) 2.8
(c)
Dose (dpa)

Fig. 3.

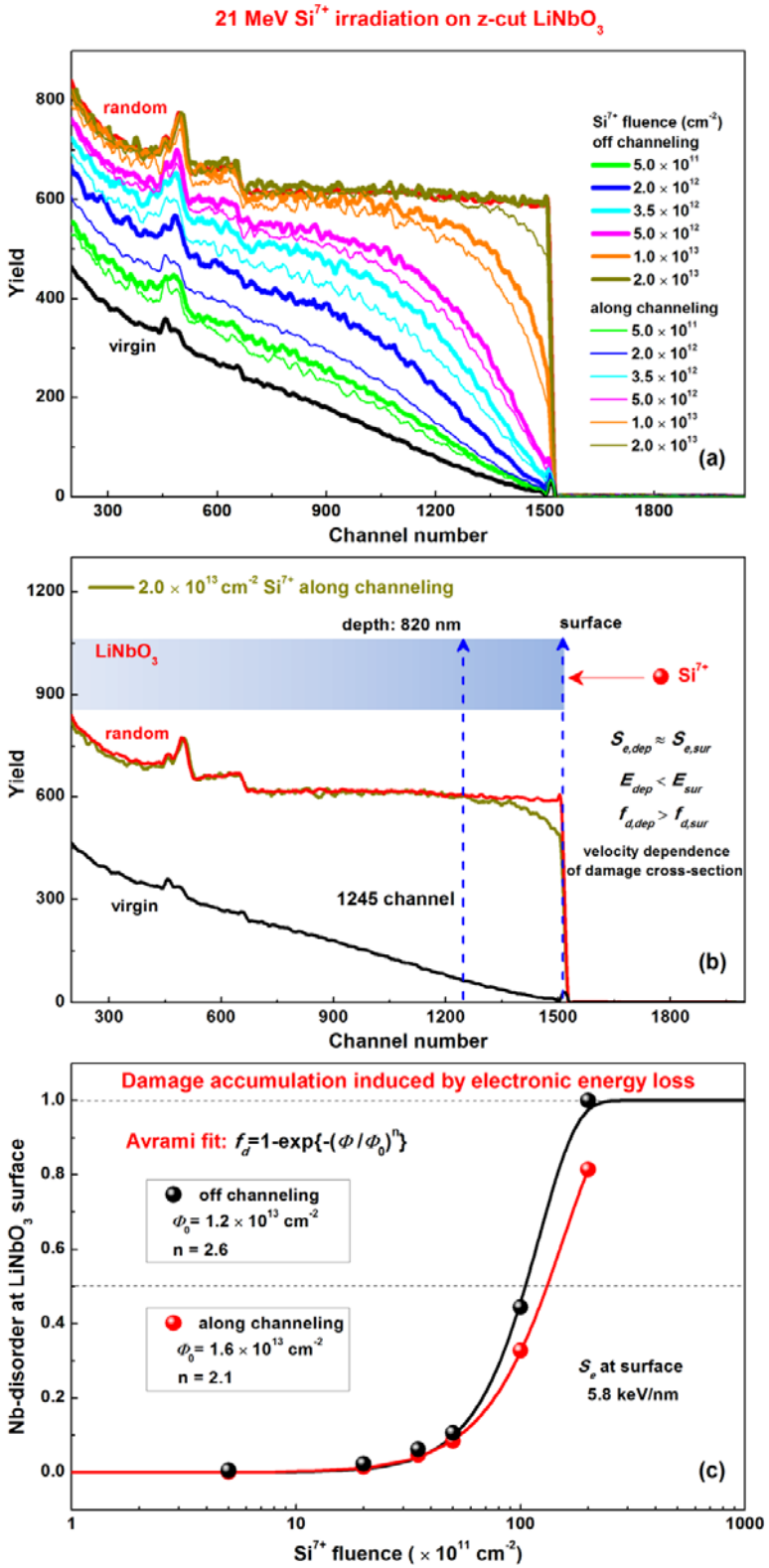
21 MeV Si7+ irradiation on z-cut LiNbO3
random
virgin
Yield
Channel number
Si7+ fluence (cm-2)
off channeling
5.0 × 10^11
2.0 × 10^12
3.5 × 10^12
5.0 × 10^12
1.0 × 10^13
2.0 × 10^13
along channeling
5.0 × 10^11
2.0 × 10^12
3.5 × 10^12
5.0 × 10^12
1.0 × 10^13
2.0 × 10^13
(a)
2.0 × 10^13 cm-2 Si7+ along channeling
depth: 820 nm
surface
LiNbO3
Si7+
random
virgin
1245 channel
Se,dep ≈ Se,sur
Edep < Esur
fd,dep > fd,sur
velocity dependence
of damage cross-section
(b)
Damage accumulation induced by electronic energy loss
Avrami fit: fd=1-exp{-(Φ/Φ0)^n}
off channeling
Φ0= 1.2 × 10^13 cm-2
n = 2.6
along channeling
Φ0= 1.6 × 10^13 cm-2
n = 2.1
Se at surface
5.8 keV/nm
Nb-disorder at LiNbO3 surface
Si7+ fluence (× 10^11 cm-2)
(c)

Fig. 4.

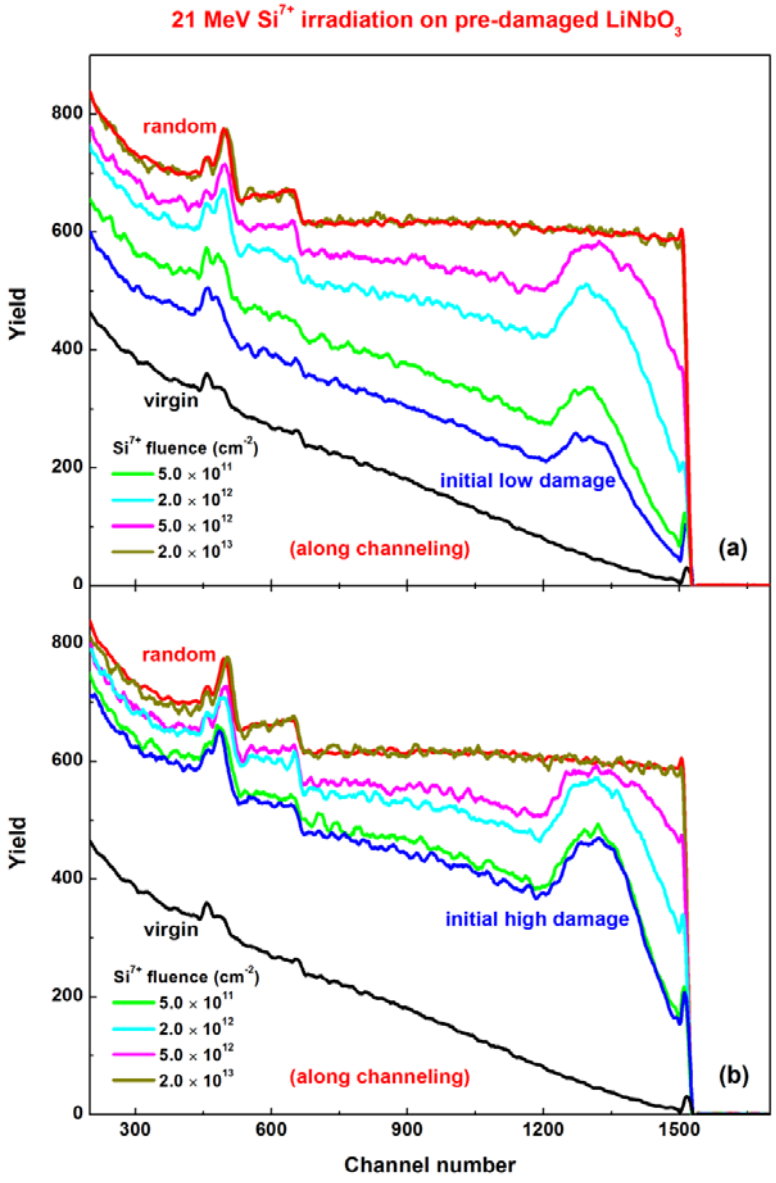
21 MeV Si7+ irradiation on pre-damaged LiNbO3
random
virgin
initial low damage
Si7+ fluence (cm-2)
5.0 × 10^11
2.0 × 10^12
5.0 × 10^12
2.0 × 10^13
(along channeling)
(a)
random
virgin
initial high damage
Si7+ fluence (cm-2)
5.0 × 10^11
2.0 × 10^12
5.0 × 10^12
2.0 × 10^13
(along channeling)
(b)
Yield
Channel number
0
200
400
600
800
300
600
900
1200
1500

Fig. 5.

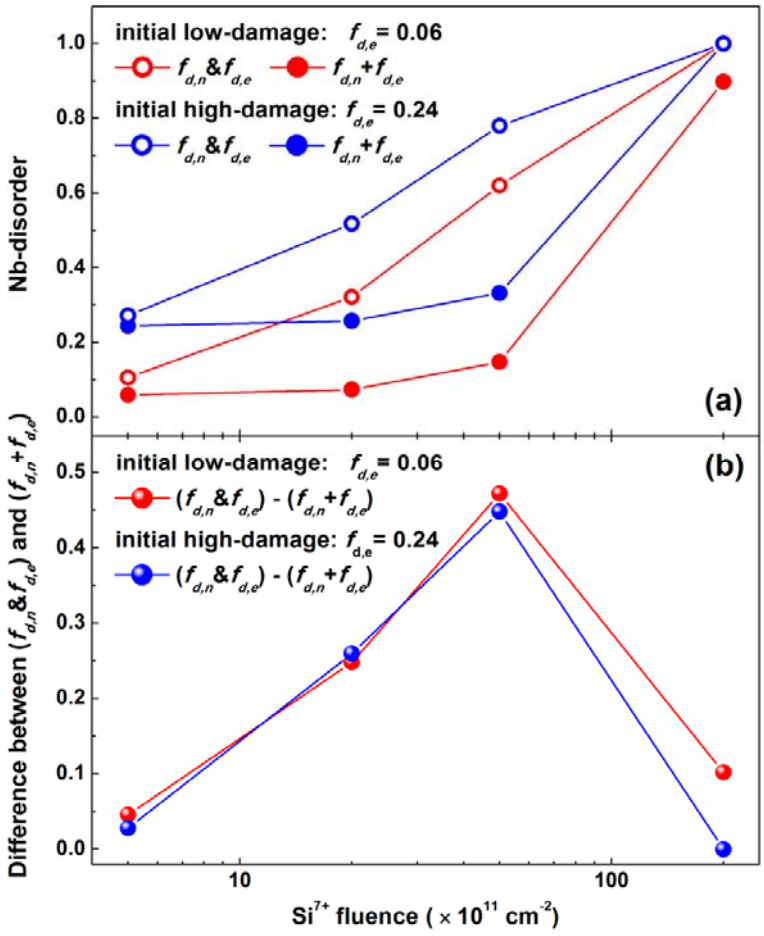
initial low-damage: $f_{d,e}$ = 0.06
$f_{d,n}$&$f_{d,e}$
$f_{d,n}$+$f_{d,e}$
initial high-damage: $f_{d,e}$ = 0.24
$f_{d,n}$&$f_{d,e}$
$f_{d,n}$+$f_{d,e}$
Nb-disorder
(a)
initial low-damage: $f_{d,e}$ = 0.06
($f_{d,n}$&$f_{d,e}$) - ($f_{d,n}$+$f_{d,e}$)
initial high-damage: $f_{d,e}$ = 0.24
($f_{d,n}$&$f_{d,e}$) - ($f_{d,n}$+$f_{d,e}$)
(b)
Difference between ($f_{d,n}$&$f_{d,e}$) and ($f_{d,n}$+$f_{d,e}$)
Si^{7+} fluence (× 10^{11} cm^{-2})